

# Polymeric Carbon Nitride/Iron Oxide Composites: A Novel Class of Catalysts with Reduced Metal Content for Ammonium Perchlorate Thermal Decomposition

Gladiya Mani, Pankajakshan Radhakrishnan Nair, and Suresh Mathew\*

Cite This: *ACS Omega* 2022, 7, 38512–38524

Read Online

ACCESS |



Metrics &amp; More

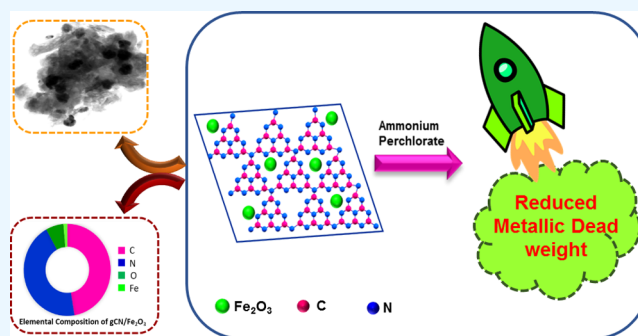


Article Recommendations



Supporting Information

**ABSTRACT:** The ever-growing number of space launches triggering an enormous release of metallic dead weight into the atmosphere has become a global concern. Despite technological advancements, the inclusion of environmental concerns in space research has become the need of the hour. Here, we report the impact of iron oxide ( $\text{Fe}_2\text{O}_3$ )-doped polymeric carbon nitride (gCN) composites with varying metal contents (namely, GF1, GF2, and GF3 with iron contents of 0.1, 0.25, and 2 mmol, respectively) as a new class of catalysts for ammonium perchlorate (AP) thermolysis. Morphology studies revealed the dendritic morphology of the synthesized  $\text{Fe}_2\text{O}_3$ , and X-ray photoelectron spectroscopy (XPS) analysis confirmed the effective interaction between  $\text{Fe}_2\text{O}_3$  and gCN in the composites. Among all of the synthesized composites, GF2 shows superior catalytic competence toward AP decomposition by amalgamating the double-stage decomposition process into a single stage followed by a considerable decrease in the decomposition temperature. The kinetic parameters calculated for the thermal decomposition of AP with and without catalysts using the KAS method substantiated the above results by significantly reducing the activation energy from 173.2 to 151.7 kJ/mol. Later, thermogravimetric and mass-spectrometric (TG-MS) analysis gives a clear idea about the catalytic efficiency of the synthesized catalyst GF2 toward AP decomposition from the accelerated emission of decomposition products  $\text{NO}$ ,  $\text{NO}_2$ ,  $\text{Cl}$ ,  $\text{HCl}$ ,  $\text{Cl}_2$ , and  $\text{N}_2\text{O}$  in the presence of GF2. In a nutshell, gCN/ $\text{Fe}_2\text{O}_3$  will open up new horizons in the field of synthesis of new catalytic systems with minimal metal content for composite solid propellants.



## INTRODUCTION

Advancements in space science and technology have made an unprecedented impact on the life of mankind. With the growing interest in human space expeditions and other space missions, the frequency of space launches is increasing exponentially every year. This rising trend in space launching accelerates the emission of a significant amount of metallic dead weight into the atmosphere. Generally, conventional metal oxide burn rate modifiers are regarded as dead weight as they remain unconsumed during propellant combustion.<sup>1</sup> Hence, the inclusion of environmental considerations in contemporary propellant research is inevitable to dodge long-term ecological impairment. Currently, great emphasis is being laid on the development of propellants that release innocuous combustion products. Even though this has been a vital global concern, ammonium perchlorate (AP) is the irreplaceable workhorse oxidizer for composite solid propellants due to its plentiful benefits including highly effective oxygen content, specific impulse, burning rate, density, and ease of handling.<sup>2,3</sup> Though ammonium nitrate is renowned as an eco-friendly green oxidizer, it has been greatly affected by polymorphism, which confines its application as a potential oxidizer.<sup>4–6</sup> Similar

efforts have been devoted to the development of chlorine-free propellants using ammonium dinitramide (ADN), hydrazinium nitroformate (HNF), and hexanitroethane (HNE) as oxidizers, but they have many limitations like high hygroscopic nature and sensitivity toward impact and friction.<sup>7</sup> Here, our effort is to upsurge the “green quotient” of propellant systems by designing new catalysts without compromising the energetics.

As the major component of propellant fuel, the thermal behavior of AP has a direct influence on the propellant performance, which has been greatly affected by various factors, namely, oxidizer particle size, the surface area of the metallic fuel, oxidizer content, and the presence of a burn rate modifier.<sup>3,8</sup> Conventionally, metal oxides are employed as burn rate modifiers and the thermal decomposition of AP is

Received: June 16, 2022

Accepted: October 6, 2022

Published: October 19, 2022



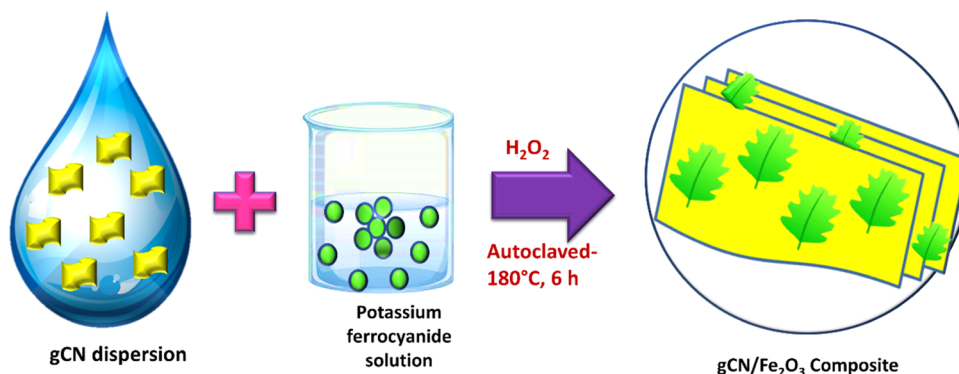


Figure 1. Schematic illustration of the synthesis of polymeric carbon nitride/iron oxide composites.

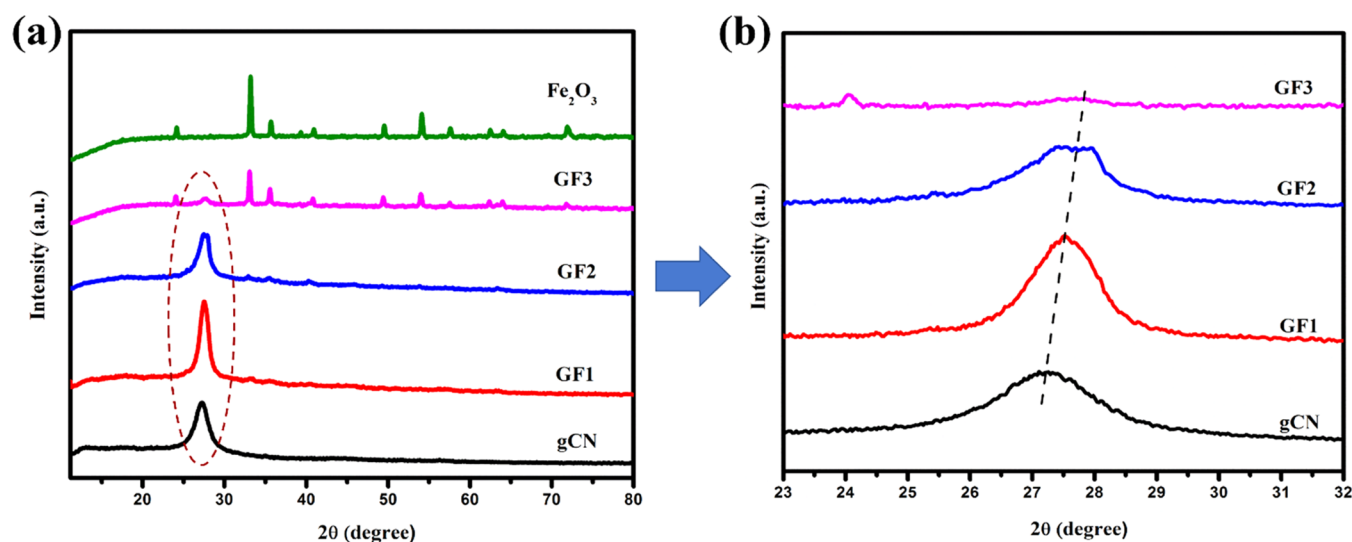


Figure 2. XRD patterns of (a) gCN,  $\text{Fe}_2\text{O}_3$ , and gCN/ $\text{Fe}_2\text{O}_3$  composites. (b) Enlarged view showing the right shift of peaks.

extremely sensitive to the presence of these metal oxide additives.<sup>9</sup> Being the most stable form of iron oxide, eco-friendly  $\alpha\text{-Fe}_2\text{O}_3$  (commonly known as hematite), an n-type semiconductor ( $E_g = 2.1$  eV), is receiving ample attention for versatile applications due to its low toxicity, abundance, high electrical conductivity, and magnetic nature.<sup>10,11</sup> Among all of the known metal oxide catalysts for propellants,  $\alpha\text{-Fe}_2\text{O}_3$  is considered one of the most studied combustion catalysts due to its low cost, positive catalytic effect, and favorable stability.<sup>12</sup> According to Kohga et al., by the addition of  $\text{Fe}_2\text{O}_3$ , a substantial increase in the burn rate value was observed by lowering the AP decomposition temperature.<sup>13</sup> Besides  $\text{Fe}_2\text{O}_3$ , ferrocene composites and metal ferrites are also being used as efficient burn rate modifiers for propellants very recently.<sup>14,15</sup> Compared to regular catalysts, nanocatalysts possess certain unique features. Besides their superior catalytic efficiency, the high surface area-to-volume ratio of these nanocatalysts makes them easy to agglomerate,<sup>16</sup> and this remains a bottleneck to good catalytic efficiency.

Hence, the use of matrices, especially two-dimensional (2D) materials such as graphene oxide (GO), reduced graphene oxide (rGO), and polymeric carbon nitride (gCN), for the synthesis of nanoparticle composites have received sufficient attention. These supports serve as a perfect platform for (1) the uniform dispersion of nanoparticles without any agglomeration and (2) their efficient stabilization. The heterogeneous catalysts thus formed possess enhanced properties compared to

homogeneous metallic catalysts like facile synthesis, easy handling, and recyclability.<sup>11,17</sup> gCN is regarded as an emerging material among the above due to its fascinating merits such as easy synthesis from low-cost materials, moderate band gap (2.7 eV), good stability, nontoxicity, and unique layered structure.<sup>18</sup> Due to the above properties, gCN has been proven as a potential burn rate modifier for the thermal decomposition of AP.<sup>19</sup> The propensity of gCN as an efficient burn rate modifier can be explored by coupling with  $\alpha\text{-Fe}_2\text{O}_3$  to form a heterogeneous catalyst for the thermal decomposition of AP. Among the various routes adopted for enhancing the catalytic efficiency of gCN, the formation of heterojunctions with metal oxides has emerged as a new class in catalysis.<sup>20</sup> Many efforts have been made to construct iron oxide-doped polymeric carbon nitride for various applications, namely, photocatalysis<sup>21</sup> and electrochemical applications.<sup>22</sup> Rather than one-dimensional (1D) or 2D architectures, three-dimensional (3D) architectures are known for their excellent features, which complement their catalytic efficiency. Dendrites are one such hyper-branched hierarchical assembly having multidimensional domains at different levels.<sup>16</sup> Often, the preparation method is said to have a telling effect on determining the features of the final product. Among various synthesis routes, the hydrothermal method is an age-old technique employed for obtaining well-crystalline products having desired characteristics without post-annealing.<sup>23</sup> Shen et al. fabricated a dendrite-structured  $\alpha\text{-Fe}_2\text{O}_3/\text{g-C}_3\text{N}_4\text{-Zr}$

scheme for CO<sub>2</sub> reduction and found that the synergy between both has enhanced the CO<sub>2</sub> reduction considerably.<sup>24</sup> To the best of our knowledge, no such efforts have been devoted to the development of hierarchical  $\alpha$ -Fe<sub>2</sub>O<sub>3</sub>-doped polymeric carbon nitride for the thermal decomposition studies of ammonium perchlorate.

The emergence of new catalyst systems that can adequately serve the quest for future energetic materials with low toxicity, high performance, easy preparation, and less pollution has become the need of the hour.<sup>25,26</sup> In the present work, we have adopted a cost-effective, facile, and scalable hydrothermal-assisted synthesis route requiring a minimal number of chemicals (Figure 1). This can be the first step toward the construction of gCN/ $\alpha$ -Fe<sub>2</sub>O<sub>3</sub> heterojunctions for the thermal decomposition studies of AP. This catalytic system will efficiently cater to the need of developing proficient catalysts with the maximum green quotient. Here, we have synthesized gCN/ $\alpha$ -Fe<sub>2</sub>O<sub>3</sub> composites with varying metal contents and evaluated their catalytic efficiency toward AP decomposition. Our findings suggest that gCN-coupled  $\alpha$ -Fe<sub>2</sub>O<sub>3</sub> composites (GF1 and GF2) exhibit superior catalytic efficiency than pure gCN and  $\alpha$ -Fe<sub>2</sub>O<sub>3</sub>. TG-coupled MS studies revealed that the synthesized catalyst with minimal metal content significantly accelerated the rate of decomposition of ammonium perchlorate, which in turn results in faster combustion of fuel in the propellant mix, thereby accelerating the burn rate. We strongly believe that this study will pave new paths for the development of new catalysts for composite solid propellants with minimal ecological impact.

## RESULTS AND DISCUSSION

The structural composition, phase purity, and crystallinity of synthesized polymeric carbon nitride, Fe<sub>2</sub>O<sub>3</sub>, and gCN/Fe<sub>2</sub>O<sub>3</sub> composites were analyzed using X-ray diffraction (XRD). The XRD patterns of gCN, Fe<sub>2</sub>O<sub>3</sub>, and gCN/Fe<sub>2</sub>O<sub>3</sub> composites are shown in Figure 2a. Two distinct peaks at 13.1 and 27.2° are observed for gCN in Figure S1. The strongest peak at 27.2° ( $d = 0.326$  nm) corresponds to the interlayer stacking of aromatic systems, indexed to the (002) facet in the graphite-like structure, while the small-angle peak at 13.1° ( $d = 0.675$  nm) presumably relates to an in-plane stacking of structural motifs, such as the hole-to-hole distance of the nitride pores in the crystals.<sup>18,19</sup> In the XRD pattern of Fe<sub>2</sub>O<sub>3</sub>, the main characteristic diffraction peaks are located at  $2\theta$  values of 24.1, 33.1, 35.6, 40.86, 49.5, 54.0, 57.6, 62.4, 64.0, and 71.9°, which match well with the (012), (104), (110), (113), (024), (116), (018), (214), (300), and (1010) crystal planes for hematite (JCPDS-No: 33-0664), respectively.<sup>27</sup> The strong and sharp peaks suggest that the obtained  $\alpha$ -Fe<sub>2</sub>O<sub>3</sub> is highly crystalline. When  $\alpha$ -Fe<sub>2</sub>O<sub>3</sub> is coupled with gCN, it is noteworthy that the crystal phases of Fe<sub>2</sub>O<sub>3</sub> do not change at all. When compared to pure gCN, after coupling with Fe<sub>2</sub>O<sub>3</sub>, the sharp peak of gCN at 27.2° shows a small shift to a high  $2\theta$  value (Figure 2b) as the concentration of the dopant increases. This kind of XRD peak shift to a higher angle and peak broadening implies the effective host–guest interaction<sup>28</sup> and reduction in stacking distance between layered structures.<sup>29</sup> This sort of guest–host interaction existing in the composites might contribute to their better catalytic efficiency toward the thermal decomposition of AP. From Figure 2b, we can see that the peak shift is maximum in the case of GF2 compared to GF1 and GF3. For sample GF3, such kind of peak shift is not so prominent. However, in gCN/Fe<sub>2</sub>O<sub>3</sub> composites, the small

diffraction peak at 13.1° of gCN disappears completely after doping. This might be due to the hindrances raised by the dopant to van der Waals and  $\pi$ – $\pi$  stacking interactions between graphitic sheets of carbon nitride during the reaction.<sup>10</sup> The diffraction peaks corresponding to Fe<sub>2</sub>O<sub>3</sub> are not visible in samples GF1 and GF2 due to the lower concentration of the dopant in the composites, while in GF3, the XRD peaks showing the presence of Fe<sub>2</sub>O<sub>3</sub> are evident. Furthermore, no other impurity peaks are observed in the XRD patterns, confirming the successful formation of gCN, Fe<sub>2</sub>O<sub>3</sub>, and gCN/Fe<sub>2</sub>O<sub>3</sub> composites.

The formation of the synthesized gCN, Fe<sub>2</sub>O<sub>3</sub>, and gCN/Fe<sub>2</sub>O<sub>3</sub> composites were further analyzed by the Fourier transform infrared spectroscopy (FT-IR) analysis. The absorptions corresponding to each functional group present are plotted and given in Figure 3. For Fe<sub>2</sub>O<sub>3</sub>, two strong

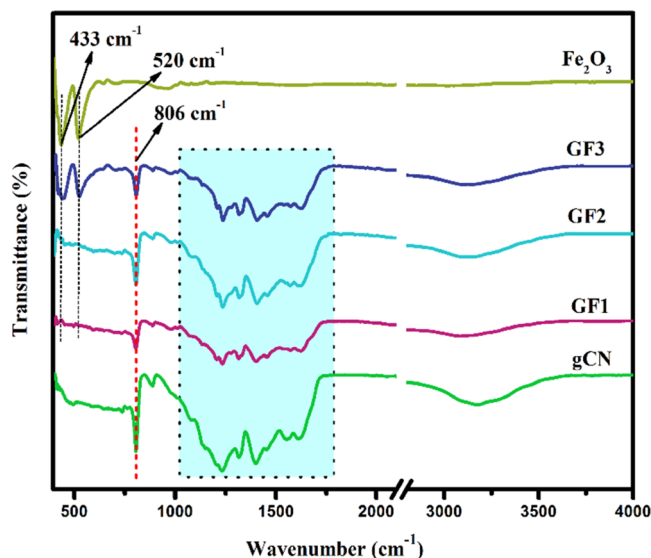


Figure 3. FT-IR spectra of gCN, Fe<sub>2</sub>O<sub>3</sub>, and gCN/Fe<sub>2</sub>O<sub>3</sub> composites.

distinct peaks at 433 and 520 cm<sup>-1</sup> were assigned to the typical stretching and bending vibrations of the Fe–O bond,<sup>30</sup> which further confirmed the formation of metal oxide. For gCN, an intense peak at 806 cm<sup>-1</sup> was attributed to the breathing mode of tri-*s*-triazine units.<sup>19</sup> The strong bands in the region of 1200–1620 cm<sup>-1</sup>, with peaks at 1231, 1319, 1398, 1446, 1550, and 1613 cm<sup>-1</sup>, were assigned to the stretching modes of the sp<sup>3</sup> C–N bond and sp<sup>2</sup> C=N heterocycles.<sup>29,31</sup> In addition to this, the broad band in the region of 3000–3500 cm<sup>-1</sup> was attributed to the presence of primary and secondary amines in carbon nitride sheets.<sup>32,33</sup> The characteristic peaks of gCN and Fe<sub>2</sub>O<sub>3</sub> were retained in all of the gCN/Fe<sub>2</sub>O<sub>3</sub> composites, confirming the formation of composites.

Further, N<sub>2</sub> adsorption–desorption isotherms for gCN, Fe<sub>2</sub>O<sub>3</sub>, and gCN/Fe<sub>2</sub>O<sub>3</sub> composites were performed to determine the Brunauer–Emmett–Teller specific surface area (BET), and the corresponding isotherms are given in Figure S2. According to Figure S2, all of the samples gCN, Fe<sub>2</sub>O<sub>3</sub>, GF1, GF2, and GF3 exhibit a type IV isotherm with a type H<sub>3</sub> hysteresis loop at high relative pressure (i.e., 0.65–1.0), revealing the presence of mesopores in the synthesized samples. The Barrett–Joyner–Halenda (BJH) method was employed to calculate the pore size distribution, and the pore diameters were found to fall in the range of 1.4–3.8 nm. The

pore size distribution confirms the presence of mesopores in samples gCN, GF1, and GF2, whereas the presence of micropores in GF3 and iron oxide.

As listed in Table 1, the specific surface areas of pure gCN and Fe<sub>2</sub>O<sub>3</sub> were 32.9 and 10.7 m<sup>2</sup>/g, respectively. After

**Table 1. Surface Parameters Obtained from N<sub>2</sub> Adsorption–Desorption Isotherms**

Sample	BET surface area (m <sup>2</sup> /g)	Avg. pore diameter (nm)	Pore volume (cm <sup>3</sup> /g)
gCN	32.9	2.5	0.19
Fe <sub>2</sub> O <sub>3</sub>	10.7	1.7	0.38
GF1	55.1	3.8	0.34
GF2	24.4	3.8	0.15
GF3	30.3	1.4	0.27

composite formation, the specific surface areas of GF1, GF2, and GF3 were found to be 55.1, 24.4, and 30.3 m<sup>2</sup>/g respectively. Even though the surface area and pore volume of GF2 is lower, the average pore diameter is higher, which may augment the adsorption of ammonia and perchloric acid molecules onto the catalyst surface. Also, the large specific surface area possessed by the catalyst is not a prerequisite for its catalytic efficiency toward AP decomposition. Similar results were obtained in our previous study.<sup>19</sup>

The morphology of a material is said to have a striking effect on defining its characteristic features, especially catalytic efficiency and optical as well as magnetic properties. Hence, the morphology of the as-prepared samples was investigated by

field emission scanning electron microscopy (FE-SEM) analysis and transmission electron microscopy (TEM) technique. Further, the elemental purity of the synthesized catalysts was examined by the energy-dispersive X-ray spectroscopy (EDX) technique and the crystalline nature of the samples was investigated using selected area electron diffraction (SAED). The low-magnification images given in Figure 4a,b depict the well-defined dendrite morphology of the synthesized Fe<sub>2</sub>O<sub>3</sub>. The dendritic fractal seems to have a hierarchical arrangement with a pronounced trunk with a length range of 3–7 μm. The highly ordered branches distributed on both sides of the trunk have lengths in the range of 1.6–2.5 μm. Furthermore, sub-branches are formed on these branches, forming another dendritic structure with a smaller size. The sub-branches are of spindle shape and are considered to be the fundamental building blocks of the entire shape.<sup>23,24</sup> The electron image of a selected area of the sample at a very low magnification chosen for EDX analysis is given in Figure 4c. The EDX investigation (Figure 4d) confirms the presence of Fe and O in the synthesized iron oxide sample, and a quantitative representation of the same is given in Figure 4e. Similarly, the FE-SEM analysis of the gCN/Fe<sub>2</sub>O<sub>3</sub> composite is given in Figure 5. The high-magnification FE-SEM images (Figure 5a,b) confirm the thin sheet-like morphology and porous nature of the synthesized gCN nanosheets. In contrast to Figure 4a,b, the dendritic structure of Fe<sub>2</sub>O<sub>3</sub> is not so evident in Figure 5a,b. According to Bharati et al., when the concentration of the precursor was high above the threshold value, diffusion of ions into the reaction medium increased and

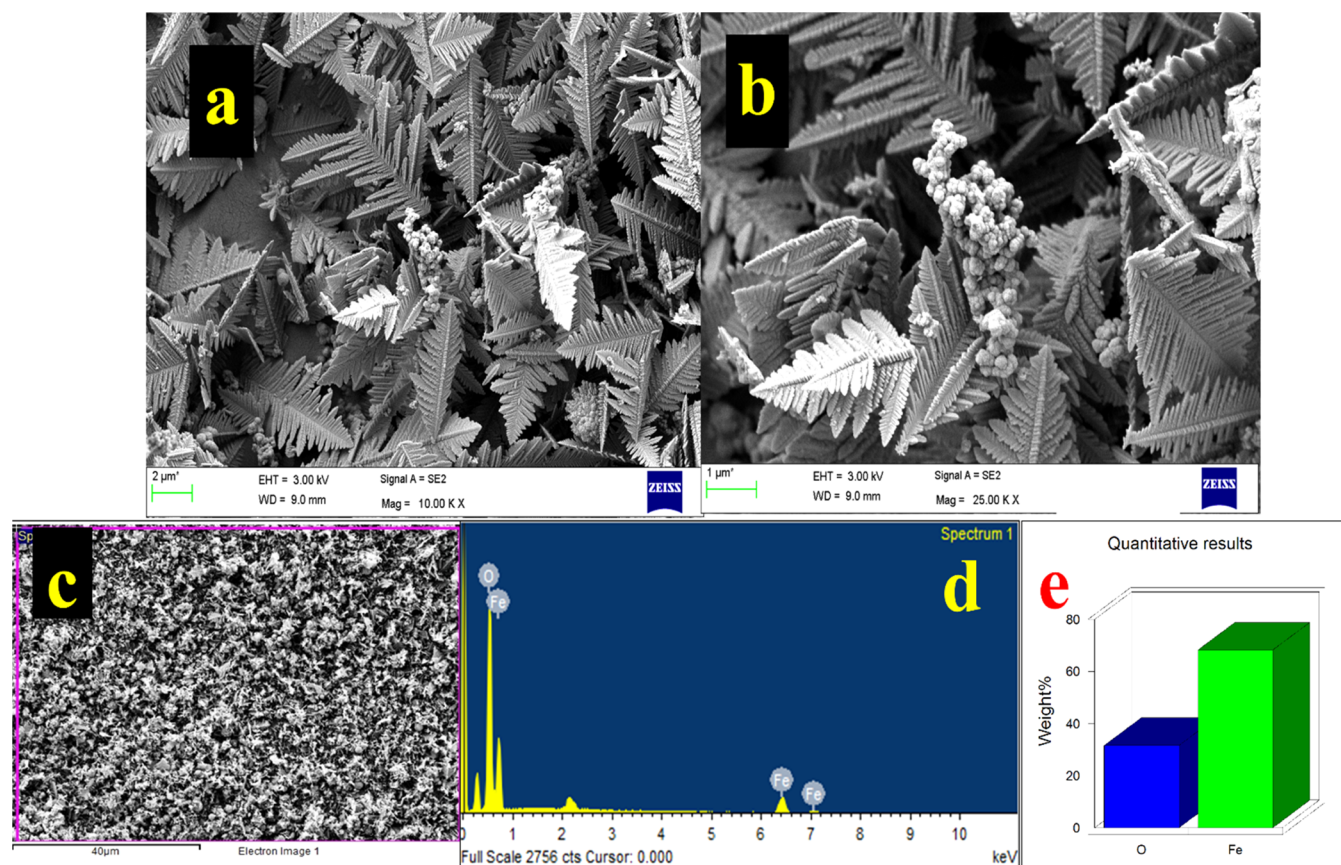


**Figure 4.** (a, b) FE-SEM images of Fe<sub>2</sub>O<sub>3</sub> with dendrite morphology. (c) Electron image of a selected area. (d) Energy-dispersive X-ray analysis (EDAX) analysis. (e) Quantitative representation of elements present in the selected area (c).

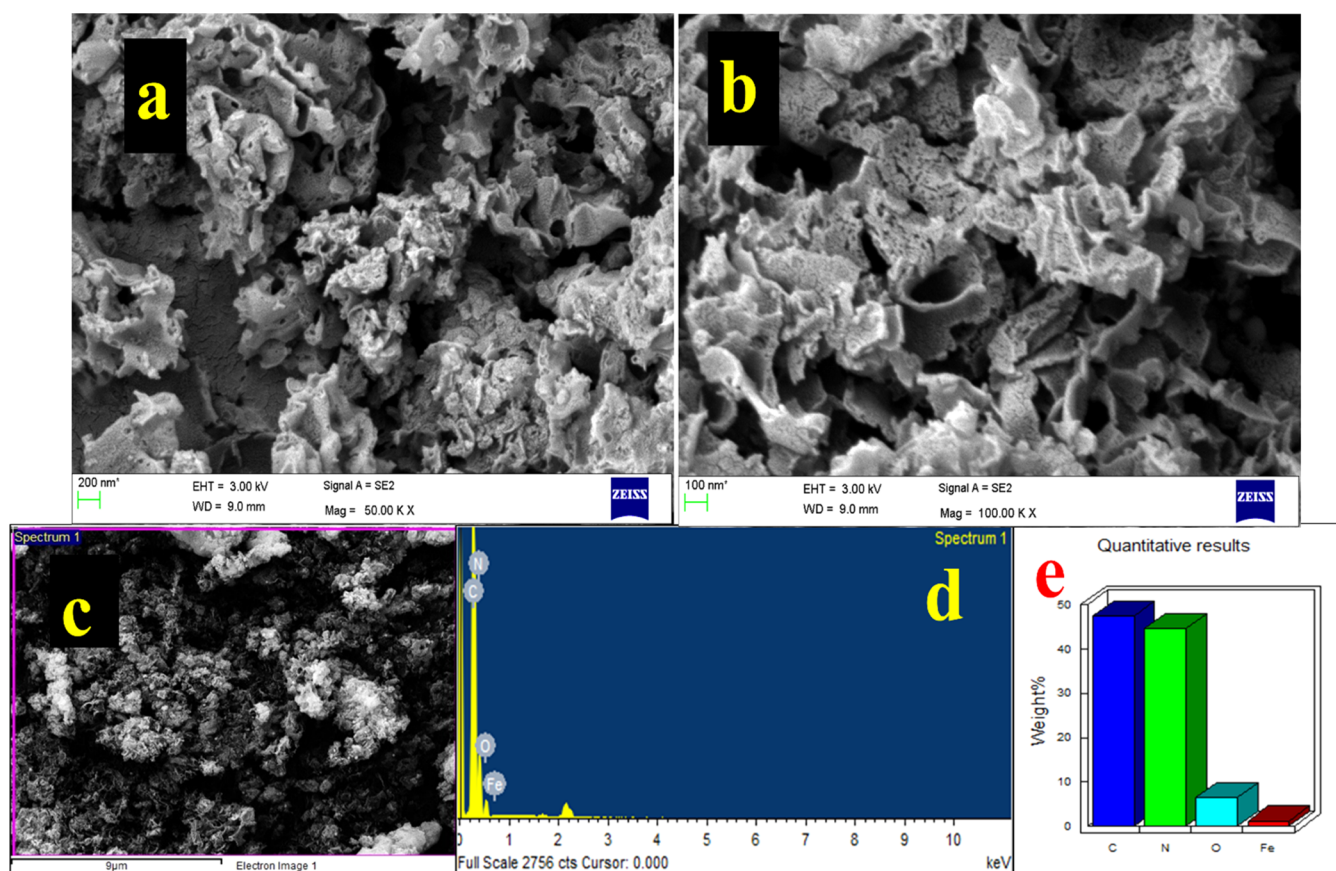


**Figure 5.** (a, b) FE-SEM images of the gCN/Fe<sub>2</sub>O<sub>3</sub> composite. (c) Electron image of a selected area. (d) EDAX analysis. and (e) Quantitative representation of elements present in the selected area (c).

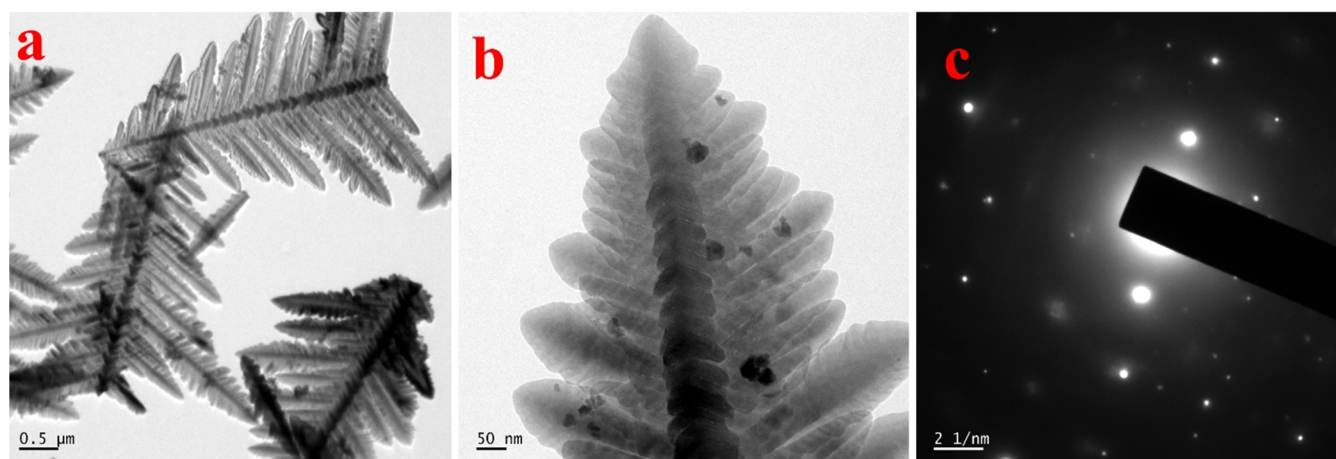


**Figure 6.** (a, b) TEM images of Fe<sub>2</sub>O<sub>3</sub> at different magnifications. (c) SAED pattern of Fe<sub>2</sub>O<sub>3</sub>.

resulted in the densification of particles, while optimizing the precursor concentration to 0.01 M, perfect dendrites were formed. Similarly, on decreasing the concentration to 0.005 M, only a part of the dendrites was formed.<sup>23</sup> In this work, when the concentration of the precursor is very small, i.e., below a threshold value, this type of failure in the formation of the dendritic structure might happen. Meanwhile, in the EDX analysis of the selected area (Figure 5c), the elements present in the sample are C, N, Fe, and O, which proves the elemental purity of the synthesized composite GF2 (Figure 5d). The intense peaks of C and N and comparatively smaller peaks of O

and Fe reveal that gCN serves as the matrix over which iron oxide is well dispersed. The quantitative representation of the elements given in Figure 5e reveals that the concentration of Fe in the composite is negligible. This also validates our findings that a minimal amount or threshold amount of the precursor is a prerequisite for the formation of the dendritic fractal.

On close observation of the TEM, high-resolution TEM (HRTEM), and SAED patterns obtained for pure Fe<sub>2</sub>O<sub>3</sub> and the gCN/Fe<sub>2</sub>O<sub>3</sub> composite, a clear idea about the crystalline nature and arrangement of particles to form a dendritic

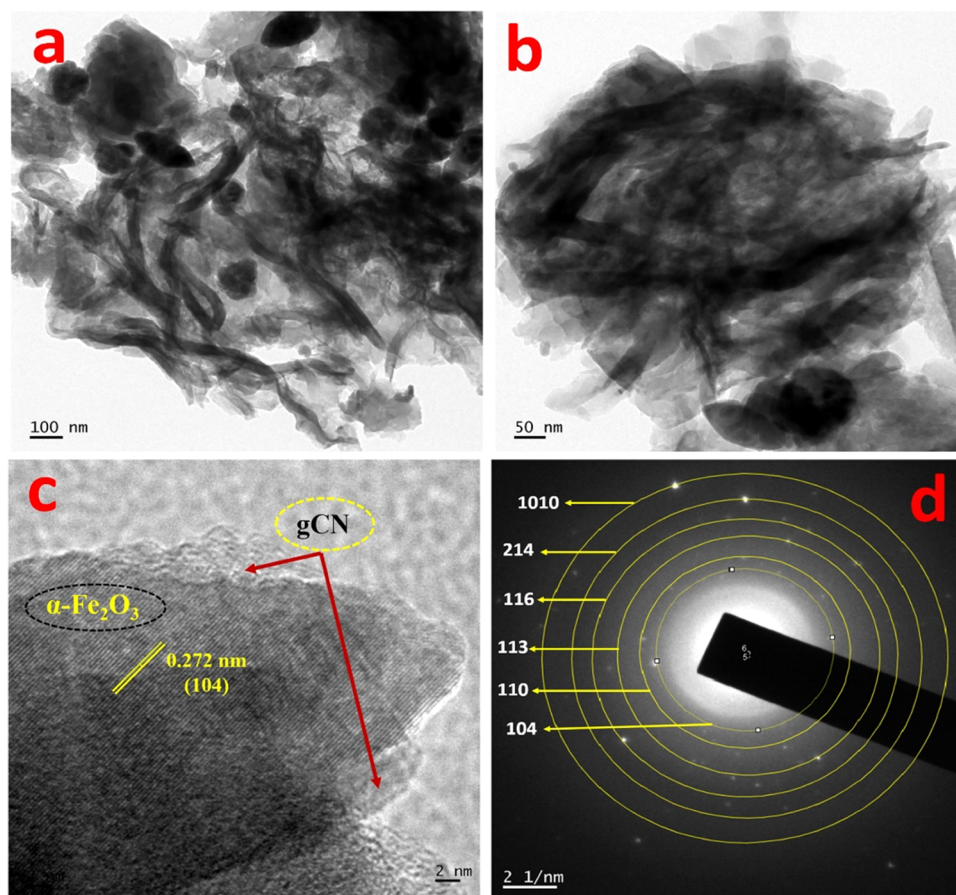


**Figure 7.** (a, b) TEM images of the gCN/Fe<sub>2</sub>O<sub>3</sub> composites at different magnifications. (c) HRTEM shows the dispersion of Fe<sub>2</sub>O<sub>3</sub> over the gCN surface. (d) SAED pattern of the composite with crystal planes corresponding to  $\alpha$ -Fe<sub>2</sub>O<sub>3</sub>.

structure can be perceived. As given in Figure 4a,b, the dendrite morphology of the synthesized Fe<sub>2</sub>O<sub>3</sub> is evident in Figure 6a,b. The high-resolution image at 50 nm discloses the captivating structure of dendrites where the trunks, branches, and sub-branches are well differentiated. According to Li et al., the hierarchical dendritic structure of synthesized Fe<sub>2</sub>O<sub>3</sub> contains steps, edges, and kinks along with twigs, which offer a plentiful amount of catalytic sites.<sup>16</sup> The SAED pattern of Fe<sub>2</sub>O<sub>3</sub> given in Figure 6c portrays the presence of bright spots, which is attributed to the crystalline nature of the synthesized sample. The TEM images of the synthesized gCN/Fe<sub>2</sub>O<sub>3</sub> composite are given in Figure 7. gCN is a 2D material with an ultrathin thickness similar to graphene. Hence, it can easily form small curling or tube-like structures during the synthesis procedure to reduce surface energy (Figure 7a,b).<sup>33</sup> Different from Figure 6a,b, the presence of Fe<sub>2</sub>O<sub>3</sub> with a dendritic structure is observed in neither Figure 7a nor Figure 7b. Instead, Fe<sub>2</sub>O<sub>3</sub> exists in an irregular morphology. As mentioned above, failure in the formation of Fe<sub>2</sub>O<sub>3</sub> dendrites is due to the lower concentration of the precursor. Even so, the HRTEM image (Figure 7c) gives strong evidence for the coexistence of both gCN and Fe<sub>2</sub>O<sub>3</sub> in the composite. The lattice fringe distance of 0.272 nm is consistent with the (104) crystal plane of  $\alpha$ -Fe<sub>2</sub>O<sub>3</sub>. The concentric rings given in Figure 7d were measured as 0.269, 0.251, 0.219, 0.169, 0.148, and 0.130 nm, which can be indexed to the (104), (110), (113), (116) (214), and (1010) crystal planes of  $\alpha$ -Fe<sub>2</sub>O<sub>3</sub>, respectively. Also, the SAED pattern of the composite shows no characteristic

diffraction rings corresponding to gCN, implying its amorphous nature.

X-ray photoelectron spectroscopy (XPS) measurements of the as-prepared samples Fe<sub>2</sub>O<sub>3</sub> and Fe<sub>2</sub>O<sub>3</sub>/polymeric carbon nitride composite (GF2) were carried out to understand the chemical composition and oxidation state of the samples. The survey spectrum given in Figure 8a suggests that the synthesized iron oxide contains iron and oxygen only. The peak corresponding to Fe 2p can be deconvoluted into four peaks with binding energies of 709.8, 715.6, 723.5, and 730.3 eV. The peaks positioned at 709.8 and 723.5 eV can be indexed to Fe 2p<sup>3/2</sup> and Fe 2p<sup>1/2</sup> states of pure  $\alpha$ -Fe<sub>2</sub>O<sub>3</sub>, respectively.<sup>34</sup> The appearance of two peaks at binding energies of 715.6 and 730.3 eV could be ascribed to the satellite peaks of Fe 2p<sup>3/2</sup> and Fe 2p<sup>1/2</sup> states of Fe<sup>3+</sup>, respectively, which confirms the formation of the  $\alpha$ -Fe<sub>2</sub>O<sub>3</sub> phase in synthesized iron oxide.<sup>35–37</sup> The O 1s spectra of Fe<sub>2</sub>O<sub>3</sub> show only two contributions, which are denoted as 528.3 and 529.1 eV. According to the literature, the peak at 528.3 eV corresponds to the presence of crystal lattice oxygen,<sup>34,38</sup> while the peak located at 529.1 eV infers the presence of oxygen vacancies or defects.<sup>39</sup> Since there is no peak observed after 531 eV, we can infer that there is no chemisorbed oxygen in the material.<sup>39</sup> In the case of the Fe<sub>2</sub>O<sub>3</sub>-doped polymeric carbon nitride composite, the survey spectrum (Figure 8b) suggests the presence of iron, oxygen, carbon, and nitrogen in the composite and provides the elemental purity of the synthesized sample.

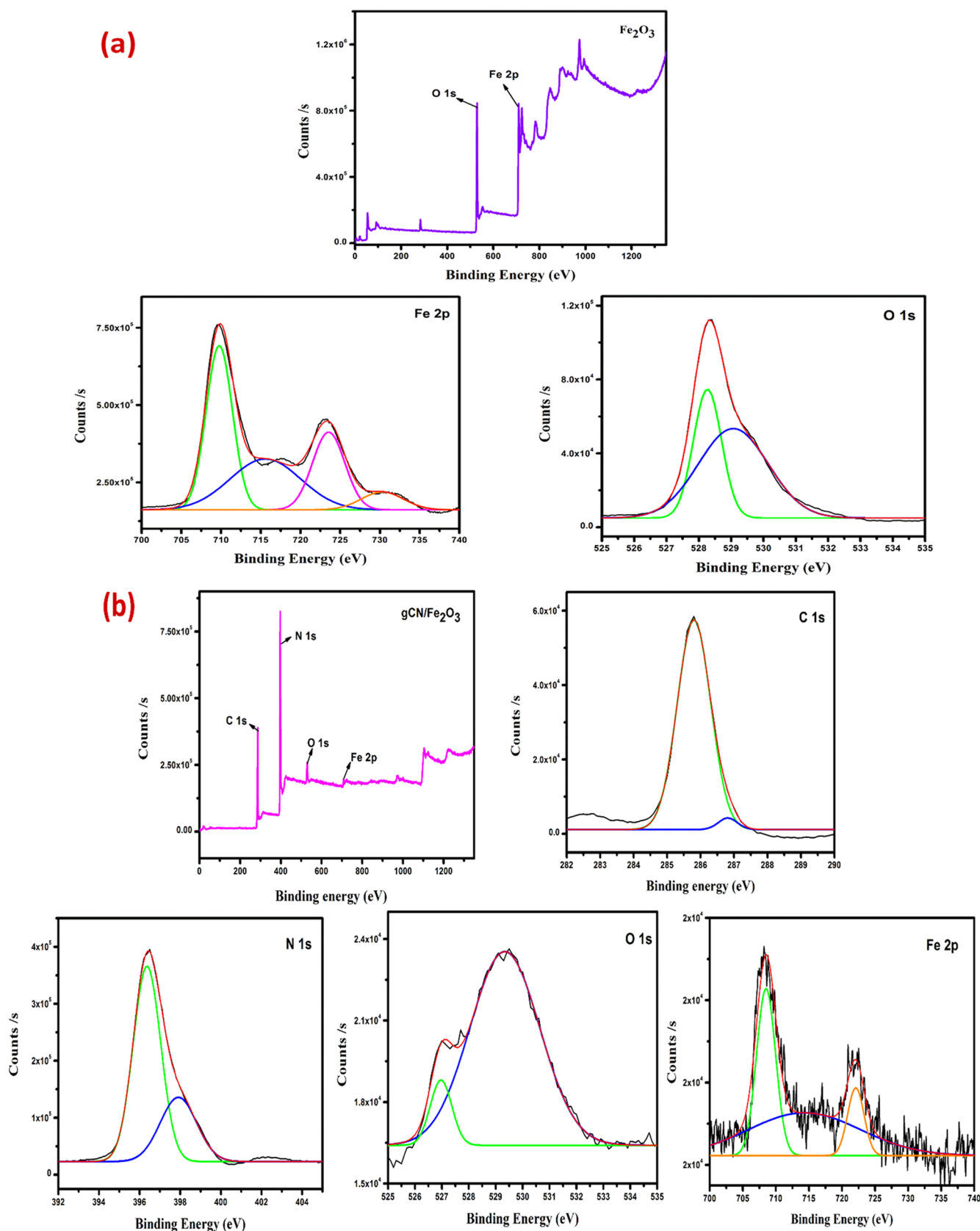


Figure 8. XPS spectra of synthesized samples: (a)  $\text{Fe}_2\text{O}_3$  and (b) gCN/ $\text{Fe}_2\text{O}_3$  composite.

According to the survey spectrum (Figure 8b), carbon and nitrogen are the major elements present in the sample (38.3 and 55.5%, respectively), while oxygen and iron are the least

present elements (5.2 and 1.1%, respectively). Hence, XPS analysis gives the quantitative interpretation of the elemental composition of sample GF2. Different from the XPS spectra of

pure  $\text{Fe}_2\text{O}_3$ , the resolved peaks of Fe 2p and O 1s in the composite show considerable variations in the peak position, inferring the influence of the chemical environment of gCN on the binding energies of Fe 2p and O 1s. Hence, the peaks of Fe 2p<sup>3/2</sup> and Fe 2p<sup>1/2</sup> shift to 708.5 and 722.1 eV, respectively. This significant shift in binding energies in the composite can be due to the effective interaction between  $\text{Fe}_2\text{O}_3$  and gCN. A similar trend of peak shifting is also found for O 1s, which again confirms the effective interaction between  $\text{Fe}_2\text{O}_3$  and gCN. Additionally, the increased area of the peak with a binding energy of 529.3 eV in the composite compared to pure  $\text{Fe}_2\text{O}_3$  shows the increased oxygen vacancy or defect in the sample. For C 1s, two deconvoluted peaks with binding energies of 285.8 and 286.8 eV are found. The strong peak at 285.8 eV can be ascribed to C–N–C coordination<sup>19</sup> originating from the tri-s-triazine units, which constitute the backbone of gCN, while the feeble peak at 286.8 eV indicates the presence of the C–OH bond.<sup>22</sup> For N 1s, peaks are positioned at 396.4 and 398.0 eV, which can be allocated to sp<sup>2</sup>-hybridized aromatic nitrogen bonded to carbon (C=N–C) and C–NH<sub>x</sub> bonds, respectively.<sup>40</sup>

The catalytic efficiencies of the as-prepared samples gCN,  $\alpha$ - $\text{Fe}_2\text{O}_3$ , and gCN/ $\text{Fe}_2\text{O}_3$  composites were extensively studied using thermal analysis techniques—thermogravimetry and differential scanning calorimetry. The TG and DTG results are shown in Figures 9 and S3, respectively. According to the

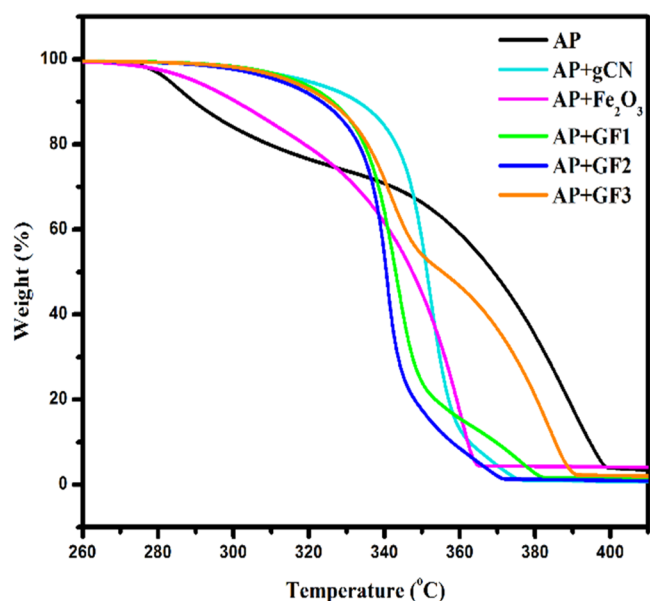


**Figure 9.** TG analysis of AP, AP + gCN, AP +  $\text{Fe}_2\text{O}_3$ , and AP + gCN/ $\text{Fe}_2\text{O}_3$  composites.

figure, the thermal decomposition of AP follows a double-stage decomposition pattern: low-temperature decomposition (LTD, below 300 °C) and a high-temperature decomposition (HTD, above 300 °C). With the addition of the catalyst, the decomposition behavior of AP changes drastically, which can be unambiguously indexed to the catalyst sensitivity of AP. For example, after the addition of gCN, the distinct two-stage decomposition mode of AP changes to almost a single-stage decomposition (Figure S3). This shift in the decomposition temperature to a lower value confirms the catalytic efficiency of gCN toward AP. Individual TG traces of AP decomposition (given in Figure 9) showing the weight loss at different stages

and temperatures at the beginning of each weight loss are given Figure S4.

Being one of the conventional catalysts for AP,  $\text{Fe}_2\text{O}_3$  performed as expected toward the AP decomposition by following a smooth decomposition curve and shifting the decomposition temperature of AP to a lower value. In the case of the composites of gCN and  $\text{Fe}_2\text{O}_3$ , sample GF2 follows almost a single-stage decomposition pattern, while GF1 and GF3 follow a double-stage decomposition pattern. Among different catalysts, the DTG peak temperature of AP (Figure S3) decreased significantly in the presence of GF2, suggesting the excellent catalytic efficiency of the composite GF2 for AP thermal decomposition. The phenomenological data of the thermogravimetric analysis of the samples with AP is given in Table 2. From DSC results (Figure 10), the AP thermal

**Table 2. Phenomenological Data of TG-DTG Analysis of AP with and without Catalysts**

sample	LTD (°C)			HTD (°C)		
	$T_i$	$T_s$	$T_f$	$T_i$	$T_s$	$T_f$
AP pure	270	285	330	330	389	400
AP + gCN	310	351	359	359	373	376
AP + $\text{Fe}_2\text{O}_3$	270	296	331	331	360	366
AP + GF1	293	343	351	351	379	382
AP + GF2	289	341	346	346	370	373
AP + GF3	294	343	351	351	384	392

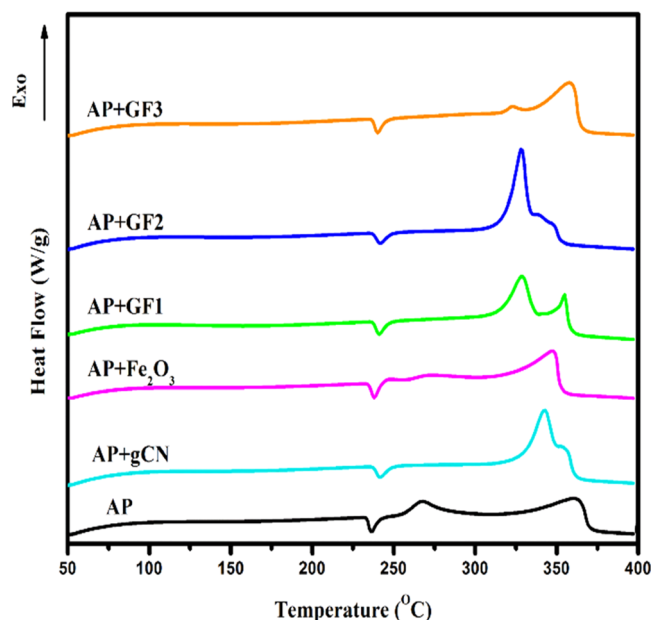


**Figure 10.** DSC analysis of AP, AP + gCN, AP +  $\text{Fe}_2\text{O}_3$ , and AP + gCN/ $\text{Fe}_2\text{O}_3$  composites.

decomposition process can be categorized into three segments: (1) a phase transition stage from orthorhombic to the cubic phase involving an endothermic peak, (2) the LTD stage, which is an autocatalytic exothermic process occurring at subsurface pores, leading to the partial decomposition of AP, and (3) the HTD stage, again an exothermic process occurring above 300 °C, results in the complete decomposition of AP.<sup>41</sup> Here, the endothermic peak indicating the phase transition of AP is centered at 236 °C. When the catalysts gCN,  $\text{Fe}_2\text{O}_3$ , and gCN/ $\text{Fe}_2\text{O}_3$  composites were added, no significant change in

the position was observed for the endothermic peak, showing that the addition of the catalyst does not affect the phase transition process. As reported earlier,  $\text{Fe}_2\text{O}_3$  is a known burn rate modifier that primarily catalyzes the HTD process in AP decomposition.<sup>41</sup> Hence, from Figure 10, a similar shift in HTD temperature was observed in the presence of  $\text{Fe}_2\text{O}_3$ , validating the above-given TG result. However, in the presence of the composites GF1, GF2, and GF3, the high-temperature decomposition peak temperature decreased and merged to a single exothermic peak in the presence of GF2, demonstrating the excellent catalytic activity of the composite GF2, whereas such kind of peak amalgamation was not spotted for the other two. In the presence of GF2, the decomposition temperature of AP decreased by 32 °C. From the thermal analyses, we can infer that among all of the synthesized catalysts, GF2 shows the maximum catalytic efficiency for AP decomposition. According to Table 1, the composite GF2 shows a higher surface area compared to  $\text{Fe}_2\text{O}_3$ . The high surface area of the composite might facilitate the faster adsorption and desorption of reactive molecules during the decomposition processes. This possibly could account for the enhanced catalytic activity of the composite. Further, enhanced surface area implies increased surface defects present on the catalyst surface, which also contribute to good catalytic activity.<sup>41</sup> Likewise, in comparing the catalytic efficiencies of pure  $\text{Fe}_2\text{O}_3$ , pure gCN, and polymeric carbon nitride-based composite GF2, GF2 shows enhanced catalytic activity toward AP decomposition, which will be an advantage for current propellant systems. Hence, polymeric carbon nitride and polymeric carbon nitride-based catalysts will be a boon to the current metallic burn rate modifiers where metallic dead weight and thus created environmental issues are usually encountered challenges.<sup>19</sup>

The catalytic behavior of sample GF2 toward AP decomposition was further studied by detailed kinetic analysis using the KAS method. For this, the TG analysis of AP and AP with the catalyst was performed at six heating rates (2, 3.5, 4, 5, 7.5, and 10 °C/min). The activation energies ( $E_a$ ) were calculated at various degrees of conversion ( $\alpha$ ) ranging from 5 to 90% using eq 1.<sup>42</sup>

$$\ln \left[ \frac{\beta}{T_\alpha^2} \right] = \ln \left[ \frac{AR}{E_a} \right] - \frac{E_a}{RT} \quad (1)$$

In the correlation, where  $\beta$  is the heating rate (K/min),  $T_\alpha$  is the temperature at a constant degree of conversion,  $A$  is the preexponential factor, and  $R$  is the universal gas constant. From the above equation, the plot of  $\ln[\beta/T_\alpha^2]$  versus  $1/T_\alpha$  would give a straight line with slope  $-E_a/R$ , from which activation energy can be calculated. The preexponential factor was also calculated from the intercept value of the above plot. The obtained values are given in Table 3. The LTD and HTD peak temperatures of AP decomposition at different heating rates are given in Table S1.

From Table 3, we can infer that in the presence of the catalyst GF2, the activation energy for the thermal

decomposition of AP decreased from 173.24 to 151.73 kJ/mol. This implies the positive catalytic efficacy of the synthesized catalyst GF2 toward AP thermal decomposition. Hence, the evaluation of kinetic parameters using the KAS method is congruent with the TG and DSC analysis findings.

Even though TG and DSC analyses give an idea about the decomposition pattern of AP with and without additives, reports concerning the amount of evolved decomposition products are scanty.<sup>19,43,44</sup> To address the above concern, here, we have made the use of the highly precise hyphenated technique—a TG-coupled MS spectrometer for the in situ analysis of evolved decomposition products. With the help of TG-MS, we could recognize the decomposition products of AP at  $m/z$  values of 30, 32, 35, 36, 44, 46, and 70 (Figure S5). The possible assignments for these fragments are  $\text{NO}^+$ ,  $\text{O}_2^+$ ,  $\text{Cl}^+$ ,  $\text{HCl}^+$ ,  $\text{N}_2\text{O}^+/\text{CO}_2^+$ ,  $\text{NO}_2^+$ , and  $\text{Cl}_2^+$ , respectively.<sup>44</sup> Along with these fragments, isotopes of  $\text{Cl}^+$ ,  $\text{HCl}^+$ , and  $\text{Cl}_2^+$  were also observed at  $m/z$  37, 38, 72, and 74, respectively, depicting the high precision of the technique used. From Figure S5, the evolved gas analysis discloses the evolution pathway of each gaseous fragment, i.e., a double-stage emission pattern corresponding to the LTD and HTD processes of AP decomposition. In the presence of the catalyst GF2, the two-stage decomposition pattern displays a tendency to get merged to a single peak, suggesting the catalytic efficacy of GF2 toward AP decomposition. Similar peak amalgamation was also observed in TG and DSC analyses. According to the literature,<sup>45</sup> AP decomposition starts with the formation of ammonia and perchloric acid gases followed by their adsorption to the AP surface. As the temperature increases, these adsorbed molecules get desorbed from the AP surface and undergo oxidation–reduction reactions. At low temperatures, the oxidation of  $\text{NH}_3$  starts with the formation of  $\text{N}_2\text{O}$  and small amounts of other gases. When the temperature increases, complete oxidation of  $\text{NH}_3$  takes place with the evolution of  $\text{NO}$ ,  $\text{N}_2\text{O}$ , and  $\text{NO}_2$  gases (Figure S5). Simultaneous acceleration in the evolution of other gaseous decomposition products such as  $\text{Cl}$ ,  $\text{HCl}$ ,  $\text{O}_2$ , and  $\text{Cl}_2$  was also observed in higher concentrations at HTD in the presence of GF2 (Figure S5). This increased concentration of decomposition products from GF2-catalyzed AP decomposition compared to pure AP implicates the effective interaction between ammonia and perchloric acid and thereby the complete decomposition of AP. Hence, from TG-MS analysis, we can conclude that the increased evolution of oxidizing species like  $\text{O}_2$ ,  $\text{NO}$ ,  $\text{HCl}$ , and  $\text{Cl}_2$  in the presence of the catalyst GF2 implies a faster rate of decomposition of AP. This accelerated decomposition suggests accelerated combustion of fuel in the propellant mix and hence an enhanced burning rate.

According to the XPS results, the presence of Fe in the composite is very minimal (1.1 atomic %). Surprisingly, with this minimal metallic content, GF2 could achieve significant catalytic efficiency. Hence, from the above results, we can say that by the use of GF2 as a catalyst for propellants, we can reduce the metallic content in burn rate modifiers substantially and thereby the release of unconsumed metallic dead weight into the atmosphere during propellant combustion. Therefore, the synthesis of an iron oxide-doped polymeric carbon nitride composite will lead the way for the evolution of more catalysts for composite solid propellants with minimal metal content. A table of comparison of the amount of metallic dead weight released during AP decomposition reported in the literature with the current study is given in Table S2.

**Table 3. Average  $E_a$  and  $A$  Values were Calculated for Thermal Decomposition of AP with and without the Catalyst Using the KAS Method**

Sample	Avg. $E_a$ (kJ/mol)	Avg. $A$ ( $\text{min}^{-1}$ )
AP	173.24	$2.6 \times 10^{16}$
AP + GF2	151.73	$7.7 \times 10^{13}$

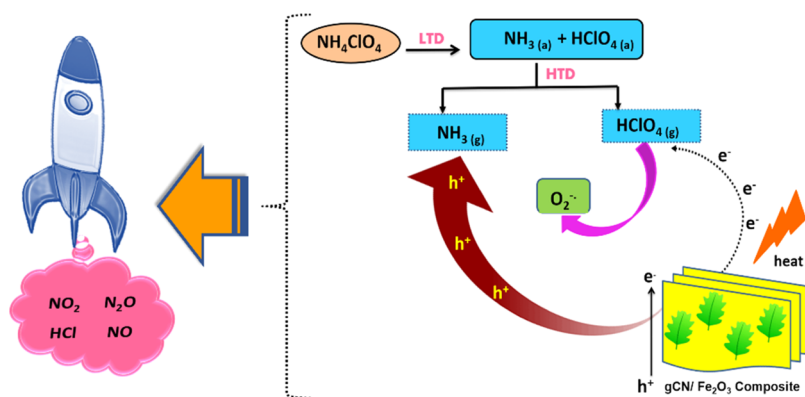


**Figure 11.** Mechanism of decomposition of AP in the presence of the catalyst  $\text{Fe}_2\text{O}_3$ -doped polymeric carbon nitride.

The thermal decomposition process of AP is a complex heterogeneous system that includes solid–gas multiphase reaction procedures such as decomposition and sublimation.<sup>46</sup> A plausible mechanism of AP thermal decomposition in the presence of the synthesized catalyst  $\text{Fe}_2\text{O}_3$ -doped polymeric carbon nitride is shown in Figure 11. According to the literature,<sup>46–49</sup> the thermal decomposition of AP follows an electron transfer process from the  $\text{ClO}_4^-$  anion to the  $\text{NH}_4^+$  cation. However, since AP is a typical dielectric, it is impossible to proceed with low-temperature decomposition via an electron transfer mechanism.<sup>45</sup> The primary products detected by various researchers were ammonia and perchloric acid, which allow the assumption that the primary stage AP decomposition follows the proton transfer mechanism. Generally, the proton transfer mechanism follows three steps: step I comprises pair of ions in an AP lattice, and step II involves the AP decomposition via proton transfer from the ammonium cation to the perchlorate anion, followed by ammonia and perchloric acid formation by molecular complex decomposition included in step III. As reported earlier, the amino groups present in the polymeric carbon nitride chains impart a Lewis base nature to gCN. During the AP decomposition process, perchloric acid molecules get adsorbed to the gCN surface via this Lewis acid–base interaction, which augments the decomposition procedure.<sup>50</sup> Similarly, due to the small band gap of gCN (2.7 eV), it is easy to form holes and electrons on the gCN surface by thermal excitation. These electrons then reduce perchloric acid into a superoxide anion during the decomposition process. This strong oxidizing agent (superoxide anions) along with the holes created during the thermal excitation then oxidizes  $\text{NH}_3$  into oxides of nitrogen such as  $\text{NO}_2$ ,  $\text{N}_2\text{O}$ , and  $\text{NO}$ .<sup>19</sup> This leads to faster decomposition of AP in the presence of gCN. Also, the catalytic effect of  $\text{Fe}_2\text{O}_3$  is said to be on the high-temperature decomposition process.<sup>51</sup> According to Fertassi et al.  $\text{Fe}_2\text{O}_3$  forms a metal complex between the metal cation  $\text{Fe}^{3+}$  and the perchlorate anion. Since these anions are electrically unstable, they tend to attract electrons from oxygen atoms in the perchlorate anion, which then leads to the dissociation of the oxygen–chlorine bond. This finally results in accelerated AP decomposition.<sup>52</sup> The presence of two additives in the form of GF2 gives better results than individual components due to its reasonable surface area, abundant active sites, and good synergy between  $\text{Fe}_2\text{O}_3$  and gCN. Hence, through this study, we are successful in developing an efficient catalyst–iron oxide-doped polymeric carbon nitride composite for propel-

lants that can proficiently address environmental concerns such as the release of metallic dead weight from propellants.

## CONCLUSIONS

Here, we have successfully synthesized polymeric carbon nitride-based iron oxide-doped catalysts with minimal metallic content via a bottom-up approach for ammonium perchlorate thermal decomposition studies. XPS analysis confirmed the effective interaction between  $\text{Fe}_2\text{O}_3$  and gCN, while the morphology studies revealed the dendritic structure of the synthesized  $\text{Fe}_2\text{O}_3$ . From surface area analysis, the larger pore size of GF2 could augment the faster adsorption of ammonia and perchloric acid molecules onto the catalyst surface. This will lead to the greater catalytic activity of GF2 toward AP thermal decomposition. Further, TG and DSC analysis techniques confirmed the enhanced catalytic efficiency of GF2 toward AP thermal decomposition by merging the double-stage decomposition process into a single stage. These results were further substantiated by kinetic analysis. In the presence of GF2, the  $E_a$  value of AP was reduced significantly (i.e., by 21.5 kJ/mol). Evolved gas analysis shows that at LTD, oxidation of  $\text{NH}_3$  starts with the formation of  $\text{N}_2\text{O}$  and small amounts of other gases. As the temperature increases, more oxidizing species get emitted, implying the faster decomposition of catalyzed AP compared to pure AP. The efficient catalytic activity of GF2 could be ascribed to the synergistic effect and presence of well-established heterojunction between pure gCN and  $\text{Fe}_2\text{O}_3$ . Hence, gCN/ $\text{Fe}_2\text{O}_3$ -based catalysts will open up new avenues in the field to formulate new catalytic systems with reduced dead weight for composite solid propellants.

## EXPERIMENTAL SECTION

**Materials and Methods.** The following chemicals were purchased and used as received. Potassium ferrocyanide (Rankem), hydrogen peroxide (Merck), urea (Spectrum), ammonium perchlorate (APEP, ISRO Aluva, Kerala, India). All of the chemicals were of analytical grade.

**Synthesis.** *Synthesis of Polymeric Carbon Nitride (gCN).* gCN was synthesized as reported earlier.<sup>19</sup> About 5 g of urea was taken in a silica crucible and heated in a muffle furnace at 530 °C for 4 h in an air atmosphere. After cooling naturally to room temperature, pale yellow-colored fluffy gCN was obtained. It was used for further analysis.

*Synthesis of Polymeric Carbon Nitride/Iron Oxide Composites.* About 0.25 g of polymeric carbon nitride was well dispersed in 100 mL of deionized water by ultrasonication

for 75 min. To this, 10 mL of potassium ferrocyanide [ $K_4Fe(CN)_6$ ] solution was added very slowly with magnetic stirring. The solution was allowed to magnetically stir for 45 min at 720 rpm. Later, a 30% solution of  $H_2O_2$  was added to the above mixture dropwise with stirring. After the addition of  $H_2O_2$ , the solution was turned from pale yellow to bright yellow, indicating the oxidation of  $Fe^{2+}$  to  $Fe^{3+}$ . This was then transferred to a Teflon beaker and autoclaved at 180 °C for 6 h. After cooling naturally to room temperature, the as-obtained product was centrifuged and washed with deionized water several times followed by ethanol. It was then dried and used for further analysis. Similarly, a series of composites of gCN and  $Fe_2O_3$  were prepared by varying the metal content. A schematic representation of the synthesis procedure is shown in Figure 1. Depending on the concentration of  $Fe_2O_3$  in the composites, the samples were named GF1 (0.1 mmol), GF2 (0.25 mmol), and GF3 (2 mmol). Pure  $Fe_2O_3$  was synthesized by the same procedure without the addition of gCN.

## ■ ASSOCIATED CONTENT

### SI Supporting Information

The Supporting Information is available free of charge at <https://pubs.acs.org/doi/10.1021/acsomega.2c03761>.

Diagrammatic representation of the results obtained from XRD, BET, DTG, TG, and TG-MS analyses and tabular representations of peak temperatures of AP decomposition at different heating rates along with a comparison with previous works reported in the open literature (PDF)

## ■ AUTHOR INFORMATION

### Corresponding Author

Suresh Mathew – School of Chemical Sciences, Mahatma Gandhi University, Kottayam, Kerala 686560, India; Advanced Molecular Materials Research Centre, Mahatma Gandhi University, Kottayam, Kerala 686560, India; [orcid.org/0000-0002-7461-3438](https://orcid.org/0000-0002-7461-3438); Email: [sureshmathewmgu@gmail.com](mailto:sureshmathewmgu@gmail.com)

### Authors

Gladiya Mani – School of Chemical Sciences, Mahatma Gandhi University, Kottayam, Kerala 686560, India; [orcid.org/0000-0003-0224-7720](https://orcid.org/0000-0003-0224-7720)

Pankajakshan Radhakrishnan Nair – Advanced Molecular Materials Research Centre, Mahatma Gandhi University, Kottayam, Kerala 686560, India

Complete contact information is available at: <https://pubs.acs.org/10.1021/acsomega.2c03761>

### Author Contributions

The manuscript was written with the contributions of all authors. All authors have approved the final version of the manuscript.

### Notes

The authors declare no competing financial interest.

## ■ ACKNOWLEDGMENTS

This work was supported by the Indian Space Research Organization RESPOND Project (Ref No: ISRO/RES/3/712/18-19). G.M. thanks the UGC, India for the fellowship. The authors are thankful to Dr. R. Rajeev for the fruitful discussion. The authors also gratefully acknowledge Vikram Sarabhai

Space Centre, Thiruvananthapuram for the DSC analysis, IUCNN, Mahatma Gandhi University, Kottayam for the TEM analysis, St. Thomas College, Pala for the XRD analysis, and School of Chemical Sciences and Advanced Molecular Materials Research Centre, Mahatma Gandhi University, Kottayam for other characterization techniques. The authors would like to thank all research students of Prof. (Dr.) Suresh Mathew for all of the discussion and support throughout this work.

## ■ REFERENCES

- (1) Chandrababu, P.; Thankarajan, J.; Nair, V. S.; Raghavan, R. Decomposition of Ammonium Perchlorate: Exploring Catalytic Activity of Nanocomposites Based on Nano Cu/Cu<sub>2</sub>O Dispersed on Graphitic Carbon Nitride. *Thermochim. Acta* **2020**, *691*, 178720–178727.
- (2) Jos, J.; Mathew, S. Ammonium Nitrate as an Eco-friendly Oxidizer for Composite Solid Propellants: Promises and Challenges. *Crit. Rev. Solid State Mater. Sci.* **2017**, *42*, 470–498.
- (3) Nair, S.; Mathew, S.; Reghunadhan Nair, C. P. Lattice Inclusion of Copper Ions in Ammonium Perchlorate through Co-crystallization: Impact on Lattice, Physical, and Thermal Characteristics. *ACS Omega* **2020**, *5*, 18544–18550.
- (4) Sudhakar, A. O. R.; Mathew, S. Thermal Behaviour of CuO Doped Phase-stabilised Ammonium Nitrate. *Thermochim. Acta* **2006**, *451*, 5–9.
- (5) Mathew, S.; Krishnan, K.; Ninan, K. A DSC Study on the Effect of RDX and HMX on the Thermal Decomposition of Phase Stabilized Ammonium Nitrate. *Propellants, Explos., Pyrotech.* **1998**, *23*, 150–154.
- (6) Mathew, S.; Eisenreich, N.; Engel, W. Thermal Analysis using X-ray Diffractometry for the Investigation of the Solid State Reaction of Ammonium Nitrate and Copper Oxide. *Thermochim. Acta* **1995**, *269–270*, 475–489.
- (7) Zhang, L. N.; Lin, Q. Q.; Cheng, B. D.; Wang, P. C.; Lu, M.; Lin, Q. H. Effect of Hexanitroethane (HNE) and Hydrazinium Nitroformate (HNF) on Energy Characteristics of Composite Solid Propellants. *FirePhysChem* **2021**, *1*, 116–122.
- (8) Yaman, H.; Çelik, V.; Değirmenci, E. Experimental Investigation of the Factors Affecting the Burning Rate of Solid Rocket Propellants. *Fuel* **2014**, *115*, 794–803.
- (9) Kapoor, I. P. S.; Srivastava, P.; Singh, G. Nanocrystalline Transition Metal Oxides as Catalysts in the Thermal Decomposition of Ammonium Perchlorate. *Propellants, Explos., Pyrotech.* **2009**, *34*, 351–356.
- (10) Babar, S.; Gavade, N.; Shinde, H.; Mahajan, P.; Lee, K. H.; Mane, N.; Deshmukh, A.; Garadkar, K.; Bhuse, V. Evolution of Waste Iron Rust into Magnetically Separable g-C<sub>3</sub>N<sub>4</sub>-Fe<sub>2</sub>O<sub>3</sub> Photocatalyst: An Efficient and Economical Waste Management Approach. *ACS Appl. Nano Mater.* **2018**, *1*, 4682–4694.
- (11) Tadic, M.; Kopanja, L.; Panjan, M.; Lazovic, J.; Tadic, B. V.; Stanojevic, B.; Motte, L. Rhombohedron and Plate-like Hematite ( $\alpha$ -Fe<sub>2</sub>O<sub>3</sub>) Nanoparticles: Synthesis, Structure, Morphology, Magnetic Properties and Potential Biomedical Applications for MRI. *Mater. Res. Bull.* **2021**, *133*, 111055–111065.
- (12) Cao, S. B.; Han, X. G.; Zhang, L. L.; Wang, J. X.; Luo, Y.; Zou, H. K.; Chen, J. F. Facile and Scalable Preparation of  $\alpha$ -Fe<sub>2</sub>O<sub>3</sub> Nanoparticle by High-gravity Reactive Precipitation Method for Catalysis of Solid Propellants Combustion. *Powder Technol.* **2019**, *353*, 444–449.
- (13) Kohga, M.; Togo, S. Influence of Iron Oxide on Thermal Decomposition Behavior and Burning Characteristics of Ammonium Nitrate/Ammonium Perchlorate-based Composite Propellants. *Combust. Flame* **2018**, *192*, 10–24.
- (14) Zhang, M.; Zhao, F.; Li, H.; Jiang, Y.; Yang, Y.; Hou, X.; Zhang, J.; Li, N. Effect of Novel Graphene-based Ferrocene Nanocomposites on Thermal Decomposition of AP. *Inorg. Chim. Acta* **2022**, *530*, 120672–120678.

- (15) Dave, P.; Thakkar, R.; Sirach, R.; Deshpande, M.; Chaturvedi, S. Effect of Nanosize Zinc Ferrite on Thermolysis of Ammonium Perchlorate. *J. Electron. Mater.* **2022**, *51*, 785–792.
- (16) Li, X.; Yu, J.; Jaroniec, M. Hierarchical Photocatalysts. *Chem. Soc. Rev.* **2016**, *45*, 2603–2636.
- (17) Jiang, L.; Fu, X.; Meng, S.; Li, J.; Xie, W.; Fan, X. Graphene Oxide-(Ferrocenylmethyl) Dimethylammonium Nitrate Composites as Catalysts for Ammonium Perchlorate Thermolysis. *ACS Appl. Nano Mater.* **2022**, *5*, 1209–1219.
- (18) Thomas, A.; Fischer, A.; Goettmann, F.; Antonietti, M.; Müller, J. O.; Schlögl, R.; Carlsson, J. M. Graphitic Carbon Nitride Materials: Variation of Structure and Morphology and their Use as Metal-free Catalysts. *J. Mater. Chem.* **2008**, *18*, 4893–4908.
- (19) Mani, G.; Jos, J.; Nair, P. R.; Mathew, S. Investigation of Kinetic Parameters for Ammonium Perchlorate Thermal Decomposition in Presence of gCN/CuO by TG-MS Analysis and Kinetic Compensation Correction. *J. Solid State Chem.* **2021**, *301*, 122301–122312.
- (20) Wang, J.; Lian, X.; Chen, S.; Li, H.; Xu, K. Effect of Bi<sub>2</sub>WO<sub>6</sub>/g-C<sub>3</sub>N<sub>4</sub> Composite on the Combustion and Catalytic Decomposition of Energetic Materials: An Efficient Catalyst with g-C<sub>3</sub>N<sub>4</sub> Carrier. *J. Colloid Interface Sci.* **2022**, *610*, 842–853.
- (21) Zhu, Z.; Yu, Y.; Dong, H.; Liu, Z.; Li, C.; Huo, P.; Yan, Y. Intercalation Effect of Attapulgite in g-C<sub>3</sub>N<sub>4</sub> Modified with Fe<sub>3</sub>O<sub>4</sub> Quantum Dots to Enhance Photocatalytic Activity for Removing 2-Mercaptobenzothiazole under Visible Light. *ACS Sustainable Chem. Eng.* **2017**, *5*, 10614–10623.
- (22) Liu, L.; Wang, M.; Wang, C. In-situ Synthesis of Graphitic Carbon Nitride/Iron Oxide-Copper Composites and their Application in the Electrochemical Detection of Glucose. *Electrochim. Acta* **2018**, *265*, 275–283.
- (23) Bharathi, S.; Nataraj, D.; Seetha, M.; Mangalaraj, D.; Ponpandian, N.; Masuda, Y.; Senthil, K.; Yong, K. Controlled Growth of Single-crystalline, Nanostructured Dendrites and Snowflakes of  $\alpha$ -Fe<sub>2</sub>O<sub>3</sub>: Influence of the Surfactant on the Morphology and Investigation of Morphology Dependent Magnetic Properties. *CrystEngComm* **2010**, *12*, 373–382.
- (24) Shen, Y.; Han, Q.; Hu, J.; Gao, W.; Wang, L.; Yang, L.; Gao, C.; Shen, Q.; Wu, C.; Wang, X.; et al. Artificial Trees for Artificial Photosynthesis: Construction of Dendrite-Structured  $\alpha$ -Fe<sub>2</sub>O<sub>3</sub>/g-C<sub>3</sub>N<sub>4</sub> Z-Scheme System for Efficient CO<sub>2</sub> Reduction into Solar Fuels. *ACS Appl. Energy Mater.* **2020**, *3*, 6561–6572.
- (25) Li, H. B.; Wang, Y.; Wei, Z.; Xia, L.; Li, Z.; Zhang, T. Alkaline Metal and Alkaline Earth Metal Salts of Di (1H-tetrazol-5-yl) Methanone (DTO): Energetic Catalysts for Ammonium Perchlorate Decomposition. *New J. Chem.* **2022**, *46*, 4462–4469.
- (26) Hao, W.; Bo, J.; Liao, L.; Luo, L.; Zhang, J.; Juan, S.; Peng, R. 1-Hydroxy-1, 2, 3, 4-tetrazole and its Transition Metal Complexes: A Family of Green High-energy Catalysts for Ammonium Perchlorate. *J. Solid State Chem.* **2022**, *308*, 122896–122901.
- (27) Pei, J.; Zhao, H.; Yang, F.; Yan, D. Graphene Oxide/Fe<sub>2</sub>O<sub>3</sub> Nanocomposite as an Efficient Catalyst for Thermal Decomposition of Ammonium Perchlorate via the Vacuum-Freeze-Drying Method. *Langmuir* **2021**, *37*, 6132–6138.
- (28) Tonda, S.; Kumar, S.; Kandula, S.; Shanker, V. Fe-doped and Mediated Graphitic Carbon Nitride Nanosheets for Enhanced Photocatalytic Performance under Natural Sunlight. *J. Mater. Chem. A* **2014**, *2*, 6772–6780.
- (29) Xavier, M. M.; George, J.; Divya, K.; Adarsh, N.; Nair, P. R.; Mathew, S. Green Synthesis of a Metal-Free 0D/2D Heterojunction: A Cost-Effective Approach. *ChemistrySelect* **2019**, *4*, 11541–11547.
- (30) Babar, S.; Gavade, N.; Shinde, H.; Gore, A.; Mahajan, P.; Lee, K. H.; Bhuse, V.; Garadkar, K. An Innovative Transformation of Waste Toner Powder into Magnetic g-C<sub>3</sub>N<sub>4</sub>-Fe<sub>2</sub>O<sub>3</sub> Photocatalyst: Sustainable e-waste Management. *J. Environ. Chem. Eng.* **2019**, *7*, 103041–103053.
- (31) Mousavi, M.; Habibi-Yangjeh, A. Magnetically Separable Ternary g-C<sub>3</sub>N<sub>4</sub>/Fe<sub>3</sub>O<sub>4</sub>/BiOI Nanocomposites: Novel Visible-light-driven Photocatalysts based on Graphitic Carbon Nitride. *J. Colloid Interface Sci.* **2016**, *465*, 83–92.
- (32) Boldys, M. J.; Müller, J. O.; Antonietti, M.; Thomas, A. Ionothermal Synthesis of Crystalline, Condensed, Graphitic Carbon Nitride. *Chem. - Eur. J.* **2008**, *14*, 8177–8182.
- (33) Ma, T. Y.; Tang, Y.; Dai, S.; Qiao, S. Z. Proton-functionalized Two-dimensional Graphitic Carbon Nitride Nanosheet: An Excellent Metal-/label-free Biosensing Platform. *Small* **2014**, *10*, 2382–2389.
- (34) Shi, X.; Li, X.; Liu, G.; Du, M.; Zhang, J.; Liu, G.; Lu, Q. NaCl-assisted Synthesis of Fe<sup>2+</sup> Self-doped Fe<sub>2</sub>O<sub>3</sub>/C<sub>3</sub>N<sub>4</sub> Nanosheets as Coefficient Fenton catalyst. *J. Mater. Sci.* **2020**, *55*, 10035–10046.
- (35) Akia, M.; Mkhoyan, K. A.; Lozano, K. Synthesis of Multiwall  $\alpha$ -Fe<sub>2</sub>O<sub>3</sub> Hollow Fibers via a Centrifugal Spinning Technique. *Mater. Sci. Eng., C* **2019**, *102*, 552–557.
- (36) Vinod, K. R.; Suresh Kumar, T. R.; Radha, R.; Balasubramaniam, M.; Balakumar, S. Enhanced Shielding Effectiveness in Nanohybrids of Graphene Derivatives with Fe<sub>3</sub>O<sub>4</sub> and  $\epsilon$ -Fe<sub>3</sub>N in the X-band Microwave Region. *Nanoscale* **2018**, *10*, 12018–12034.
- (37) Luo, Y.; Tao, M.; Deng, J.; Zhan, R.; Guo, B.; Ma, Q.; Aslam, M. K.; Qi, Y.; Xu, M. Nanocubes Composed of FeS<sub>2</sub>@C Nanoparticles as Advanced Anode Materials for K-ion Storage. *Inorg. Chem. Front.* **2020**, *7*, 394–401.
- (38) Narasimman, S.; Balakrishnan, L.; Alex, Z. Fiber Optic Magnetic Field Sensor using Co Doped ZnO nanorods as Cladding. *RSC Adv.* **2018**, *8*, 18243–18251.
- (39) Mahala, C.; Basu, M. Nanosheets of NiCo<sub>2</sub>O<sub>4</sub>/NiO as Efficient and Stable Electrocatalyst for Oxygen Evolution Reaction. *ACS Omega* **2017**, *2*, 7559–7567.
- (40) Yang, Y.; Chen, J.; Mao, Z. Y.; An, N.; Wang, D. J.; Fahlman, B. Ultrathin g-C<sub>3</sub>N<sub>4</sub> Nanosheets with an Extended Visible-light-responsive Range for Significant Enhancement of Photocatalysis. *RSC Adv.* **2017**, *7*, 2333–2341.
- (41) Chandru, R. A.; Patel, R. P.; Oommen, C.; Raghunandan, B. Initial Studies on development of High-performance Nano-structured Fe<sub>2</sub>O<sub>3</sub> Catalysts for Solid Rocket Propellants. *J. Mater. Eng. Perform.* **2019**, *28*, 810–816.
- (42) Blaine, R. L.; Kissinger, H. E. Homer Kissinger and the Kissinger equation. *Thermochim. Acta* **2012**, *540*, 1–6.
- (43) Sivadas, D. L.; Thomas, D.; Haseena, M.; Jayalatha, T.; Krishnan, G. R.; Jacob, S.; Rajeev, R. Insight into the catalytic thermal decomposition mechanism of Ammonium Perchlorate. *J. Therm. Anal. Calorim.* **2019**, *138*, 1–10.
- (44) Zhu, Y. L.; Huang, H.; Ren, H.; Jiao, Q. J. Kinetics of Thermal Decomposition of Ammonium Perchlorate by TG/DSC-MS-FTIR. *J. Energy Mater.* **2014**, *32*, 16–26.
- (45) Boldyrev, V. V. Thermal Decomposition of Ammonium Perchlorate. *Thermochim. Acta* **2006**, *443*, 1–36.
- (46) Zhang, M.; Zhao, F.; Yang, Y.; An, T.; Qu, W.; Li, H.; Zhang, J.; Li, N. Catalytic Activity of Ferrates (NiFe<sub>2</sub>O<sub>4</sub>, ZnFe<sub>2</sub>O<sub>4</sub> and CoFe<sub>2</sub>O<sub>4</sub>) on the Thermal Decomposition of Ammonium Perchlorate. *Propellants, Explos., Pyrotech.* **2020**, *45*, 463–471.
- (47) Wang, W.; Zhang, D. Facile preparation of rGO/MFe<sub>2</sub>O<sub>4</sub> (M = Cu, Co, Ni) Nanohybrids and its Catalytic Performance During the Thermal Decomposition of Ammonium Perchlorate. *RSC Adv.* **2018**, *8*, 32221–32230.
- (48) Chen, J.; He, S.; Liu, Y.; Qiao, Z.; Huang, B.; Li, X.; Hao, Q.; Huang, H.; Yang, G. Highly Active Catalysts Based on 3D Hierarchically Ordered Porous Carbon with Entrapped Fe<sub>2</sub>O<sub>3</sub> Nanoparticles for the Thermal Decomposition of Ammonium Perchlorate. *Appl. Surf. Sci.* **2021**, *538*, No. 148148.
- (49) Zhang, M.; Zhao, F.; Yang, Y.; Zhang, J.; Li, N.; Gao, H. Effect of rGO-Fe<sub>2</sub>O<sub>3</sub> Nanocomposites Fabricated in Different Solvents on the Thermal Decomposition Properties of Ammonium Perchlorate. *CrystEngComm* **2018**, *20*, 7010–7019.
- (50) Li, Q.; He, Y.; Peng, R. Graphitic Carbon Nitride (gC<sub>3</sub>N<sub>4</sub>) as a Metal-free Catalyst for Thermal Decomposition of Ammonium Perchlorate. *RSC Adv.* **2015**, *5*, 24507–24512.

(51) Joshi, S. S.; Patil, P. R.; Krishnamurthy, V. Thermal Decomposition of Ammonium Perchlorate in the Presence of Nanosized Ferric Oxide. *Def. Sci. J.* **2008**, *58*, 721–727.

(52) Fertassi, M. A.; Liu, Q.; Li, R.; Liu, P.; Liu, J.; Chen, R. R.; Liu, L.; Wang, J. Ex situ Synthesis of G/ $\alpha$ -Fe<sub>2</sub>O<sub>3</sub> Nanocomposite and its Catalytic Effect on the Thermal Decomposition of Ammonium Perchlorate. *Bull. Mater. Sci.* **2017**, *40*, 691–698.